Journal of the Optical Society of America B
OPTICAL PHYSICS

Sub-kilohertz excitation lasers for quantum information processing with Rydberg atoms

REMY LEGAIE, CRAIG J. PICKEN, AND JONATHAN D. PRITCHARD*

Department of Physics, SUPA, Strathclyde University, Glasgow G4 0NG, UK
**Corresponding author: jonathan.pritchard@strath.ac.uk*

Received 21 December 2017; revised 11 February 2018; accepted 25 February 2018; posted 26 February 2018 (Doc. ID 318054); published 22 March 2018

Quantum information processing using atomic qubits requires narrow linewidth lasers with long-term stability for high-fidelity coherent manipulation of Rydberg states. In this paper, we report on the construction and characterization of three continuous-wave narrow linewidth lasers stabilized simultaneously to an ultra-high finesse Fabry–Perot cavity made of ultra-low expansion glass, with a tunable offset-lock frequency. One laser operates at 852 nm, while the two locked lasers at 1018 nm are frequency doubled to 509 nm for excitation of ^{133}Cs atoms to Rydberg states. The optical beat note at 509 nm is measured to be 260(5) Hz. We present measurements of the offset between the atomic and cavity resonant frequencies using electromagnetically induced transparency for high-resolution spectroscopy on a cold atom cloud. The long-term stability is determined from repeated spectra over a period of 20 days, yielding a linear frequency drift of ∼1 Hz/s.

OCIS codes: (020.5780) Rydberg states; (140.0140) Lasers and laser optics; (140.3425) Laser stabilization; (140.3515) Lasers, frequency doubled; (140.3600) Lasers, tunable; (140.4780) Optical resonators.
https://doi.org/10.1364/JOSAB.35.000892

1. INTRODUCTION

The field of quantum information processing (QIP) is an intensive research area. Its attractiveness lies in the possibility of speeding up classical problems and modeling complex quantum systems [1]. Neutral atoms present an attractive candidate for scalable QIP [2,3] combining long coherence times of weakly interacting hyperfine ground states [4] with strongly interacting Rydberg states [5] to create pair-wise entanglement [6,7], perform deterministic quantum gates [8,9], and even realize a quantum simulator for Ising models [10]. Rydberg excitation is typically performed using two-photon excitation due to weak single photon matrix elements from the ground state [11] and inconvenient UV wavelengths. Using a resonant two-photon excitation, Rydberg electromagnetically induced transparency (EIT) [12] can be exploited for laser frequency stabilization [13] as well as precision metrology of Rydberg state energies [14,15] and lifetimes [16], dc electric fields [17], and RF field sensors operating at both microwave [18,19] and terahertz (THz) [20] frequency ranges. For dense cold atom samples, the strong atomic interactions can be mapped onto the optical field to create non-linearities at the single photon level [21–24].

For robust Rydberg excitation of atomic qubits for gate operations the two-photon excitation must be detuned from the intermediate excited state to avoid losses due to spontaneous emission. High-fidelity gates also require narrow linewidth excitation lasers with excellent long-term frequency stability [25]. These requirements can be met using lasers stabilized to a high-finesse optical cavity [26,27], exploiting techniques developed for lasers on state-of-the-art optical lattice clocks operating at fractional instabilities $<10^{-18}$ [28,29] requiring sub-hertz (sub-Hz) laser linewidths [30–32]. Using cavities made of ultra-low expansion (ULE) glass enables minimization of the long-term drifts to <0.1 Hz/s [30], rivaled only by the performance of cryogenically cooled single crystal silicon cavities [33,34].

Recently, details of cavity stabilized laser systems for Rydberg excitation of K [35], Rb [36], and Sr [37] have been presented, achieving typical linewidths around 1–10 kHz. In this paper, we describe the stabilization of three continuous-wave lasers to a ULE reference cavity for Rydberg excitation of Cs, offering sub-kilohertz (sub-kHz) linewidths for implementation of QIP Rydberg protocols. We determine a lock bandwidth of 1.1 MHz via observation of the in-loop power spectrum. High-resolution EIT spectroscopy of cold Cs Rydberg states is used to calibrate the cavity mode frequencies with respect to Rydberg transitions and determine the cavity long-term drift ∼1 Hz/s.

2. LASER SOURCES

We perform Rydberg excitation via the Cs D_2 line using transitions from $6s^2S_{1/2} \rightarrow 6p^2P_{3/2} \rightarrow n\ell^2L_j$, as shown in Fig. 1(a). The first step of the excitation from $6s^2S_{1/2} \rightarrow 6p^2P_{3/2}$ is performed using an extended-cavity diode laser (ECDL) at 852 nm, as shown in Fig. 1(b). For the second step, light at 509 nm is required, which is generated from a pair of homebuilt second-harmonic generation (SHG) systems, Rydberg A and B, which double light from a pair of master lasers operating at 1018 nm, as shown in Fig. 1(c).

Our ECDL design uses laser diodes mounted in a solid aluminum body with frequency control achieved using holographic gratings operated in a Littrow configuration [38]. The grating mount is doubly hinged to provide decoupling of horizontal and vertical adjustment. Coarse frequency tuning of the grating angle is performed using a precision 170 TPI screw, with fine tuning achieved using a piezoelectric actuator (Thorlabs AE0505D08F). All the lasers are temperature stabilized to <0.1°C using a commercial Arroyo 5240 temperature controller driving a Peltier cooler and placed in a perspex box with an anti-reflection coated window to provide thermal and mechanical insulation.

The first step laser, Qubit A, uses a standard Fabry–Perot laser diode (Thorlabs L852P150) with 30% optical feedback from a grating with 1800 lines/mm (Thorlabs GH13-18V) giving a mode-hop free tuning range of 5 GHz. After the isolator, light passes through a noise-eater acousto-optic modulator (AOM) to eliminate intensity noise followed by a double-pass 80 MHz AOM for control of frequency and intensity before being delivered to the experiment via a polarization-maintaining (PM) single-mode optical fiber.

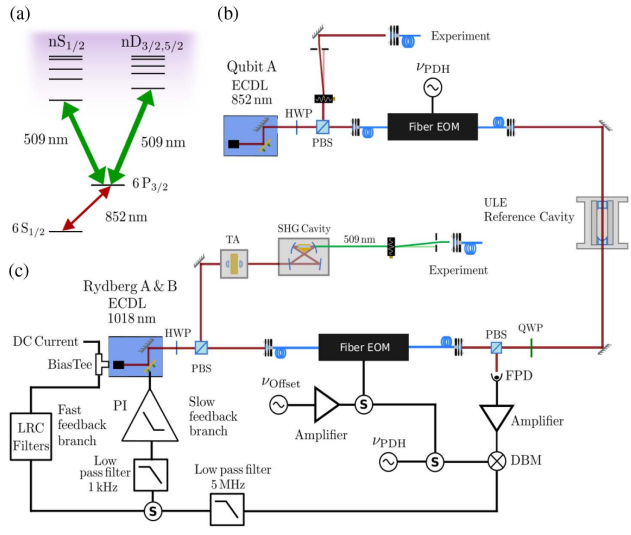

Fig. 1. (a) Schematic of the two-photon excitation of ^{133}Cs to $nS_{1/2}$ or $nD_{3/2,5/2}$ Rydberg state via $6P_{3/2}$ state. (b) Laser setup for Qubit A at 852 nm driving transition from $6S_{1/2} \rightarrow 6P_{3/2}$. (c) Locking electronics for frequency-doubled Rydberg lasers A and B driving the second stage transition at 509 nm. Key: PBS, polarizing beam splitter; HWP, half-wave plate; QWP, quarter-wave plate; FPD, fast photodiode; DBM, double balanced mixer; S, splitter; PI, proportional integral; TA, tapered amplifier; AOM, acousto-optic modulator; EOM, electro-optic modulator.

The master lasers for Rydberg A and B, are generated from AR-coated infrared laser diodes at 1018 nm (Toptica LD-1020-0400-2 and Sacher SAL-1030-060, respectively) combined with a 1200 lines/mm visible grating (Thorlabs GH13-12V) tunable from 1010 to 1025 nm with no realignment of the vertical feedback. High power is achieved using a tapered amplifier (TA) (M2K TA-1010-2000-DHP) for each laser. We obtain 1.36 W output TA power for 22 mW seed power at a TA input current of 4A.

To generate light at 509 nm, the Rydberg lasers are doubled via cavity-enhanced SHG [39] using an AR-coated quasi-phase-matched periodically poled KTP crystal from Raicol Crystal Ltd. with dimensions of $1 \times 2 \times 20$ mm and a poling period of $\Lambda = 7.725$ μm. The non-linear crystal is placed into a brass heating block at the center of a symmetrical bow-tie cavity, with temperature control provided using a Peltier device allowing temperature tuning from 15°C to 95°C. This corresponds to peak doubling efficiencies from 1020 to 1015 nm to enable excitation of Rydberg states with principal quantum number from $n \geq 45$ to ionization. The bow-tie cavity consists of two concave mirrors with −30 mm radius of curvature and two plane mirrors, designed to achieve the optimal Boyd–Kleinmann waist of 25 μm in the crystal [40]. The cavity has a free-spectral range (FSR) of 1.25 GHz and a finesse of $\mathcal{F} \sim 50$, to which we achieve 95% mode matching to the light from the TA.

The cavity length is stabilized to give peak SHG output power using the Hänsch–Couillaud technique [41], with a single proportional-integral (PI) servo feeding back to a ring piezo attached to one of the planar cavity mirrors. Following optimization of the alignment and crystal temperature, we typically obtain 370 mW at 509 nm for 650 mW infrared power, achieving ∼57% conversion efficiency at a TA current of 3.0 A. At higher infrared input powers (>1 W), we observe power clamping arising from a competing $\chi^{(2)}$—non-linearity whereby the intracavity second-harmonic beam acts as a pump for non-degenerate optical parametric oscillation [42]. This can be overcome using a lower input coupler reflectivity [43] or by adjusting the cavity geometry to increase the waist in the crystal [44]. Finally, the green light is then sent through an 80 MHz AOM to provide intensity control and coupled into a single-mode PM fiber, leading to ∼160 mW available at the cold atoms. AOM frequencies for all lasers are derived from a common direct digital synthesis (DDS) evaluation board (AD9959) device to provide controllable relative phase between the lasers.

3. LASER FREQUENCY STABILIZATION

Laser stabilization is performed by locking each of the master lasers above to a stable high-finesse reference cavity using the Pound–Drever–Hall (PDH) technique [45,46]. The reference cavity is a 10 cm cylindrical cavity from Advanced Thin Films in a plano–concave configuration with −50 cm radius of curvature. Both the mirrors and the spacer are made of ULE glass, making it possible to minimize thermal expansion of the cavity due to a zero-crossing of the linear coefficient of thermal expansion (CTE) [47] providing long-term frequency stability.

The mirror substrates have a dual-wavelength coating to provide high finesse at both 852 nm and 1018 nm simultaneously.

The optical reference cavity is housed in an evacuated vacuum chamber to minimize fluctuations in cavity frequency due to changes in the refractive index. Using the 3-l/s ion pump on the cavity chamber, we maintain a pressure of 3×10^{-7} mbar. The cavity is mounted horizontally on a pair of Viton O-rings placed at the Airy points [48] to reduce sensitivity to vibration. The vacuum chamber is externally temperature-stabilized using a PI temperature controller that drives a current through heater tapes connected in parallel and wound around the cavity vacuum chamber, itself surrounded by 1 cm thick foam insulation. For passive vibration isolation, the cavity is mounted on a 60 × 60 cm^2 breadboard that rests on a layer of Sorbothane on a floating optical table. Further improvements could be achieved using a radiation shield around the cavity in vacuum or enclosing the cavity setup within a second stage of temperature control [30].

The optical setup for laser locking is shown in Fig. 2. We pick off ∼1 mW of light from each ECDL and couple the light into fiber-coupled electro-optic phase modulators (EOMs) (Jenoptik Models PM-830 and PM-1064) for generating sidebands on the light. The fiber EOMs provide broadband phase modulation (up to 5 GHz) while minimizing residual amplitude modulation and cleaning the mode shape and the polarization incident on the cavity. Due to the high insertion loss of the modulators, this leaves around 200 μW available for laser stabilization, which is mode-matched into the cavity using lenses $f_{1,2}$ to maximize coupling to the TEM_{00} cavity mode. Light from the two Rydberg master lasers (A and B) is combined on a polarizing beam splitter (PBS) with orthogonal polarization and coupled into the cavity using a dichroic mirror (DM) to separate the incident 1018 nm light from the transmitted 852 nm light from the cavity. To isolate the reflected signal for cavity locking, 50:50 beam splitters are placed in each beam path prior to the PBS allowing independent detection photodiodes to be used. Similarly, after the cavity a second DM and PBS are used to separate the transmission signals of the two Rydberg lasers. Finally, the transmitted and reflected signals from the cavity are monitored via a high-gain and a high-bandwidth home-built photodiodes, respectively. The high-gain photodiode has been optimized for ring-down measurements on the ULE cavity, with a total gain of 2.5×10^6 V/A and a measured roll-off frequency of $F_{-3\,dB} = 890$ kHz. The high-bandwidth photodiode uses a fast photodetector (Hamamatsu S5971) with a single gain stage to provide a bandwidth of 25 MHz and a gain of 5×10^4 V/A. Electronics for the PDH lock are shown schematically in Fig. 1(c). Each EOM is driven by a low-frequency signal (ν_{PDH}) at +10 dBm to generate first-order sidebands with 10% amplitude (phase modulation index $\delta = 0.7$ rad). To minimize cross talk between lasers, frequencies of $\nu_{PDH} = 8.4, 10, 11.7$ MHz are chosen, ensuring any interference effects occur at beat frequencies above the servo bandwidth. The PDH error signal is obtained by first amplifying the signal from the reflection photodiode using a low-noise amplifier and then demodulating at ν_{PDH} on a mixer followed by a low-pass filter at 5 MHz. After the filter, the error signal is split into two simultaneous feedback branches to the laser. The first provides fast feedback directly to the diode laser current using a resistor for direct feedback in parallel with passive phase-advance and phase-delay filters as detailed in [26]. This is combined with the laser drive current using a bias-tee, and filter component values optimized to maximize the achievable servo bandwidth. A second, low-frequency PI servo loop (DC-300 Hz) provides feedback to the laser piezo to ensure the laser remains locked to the cavity peak.

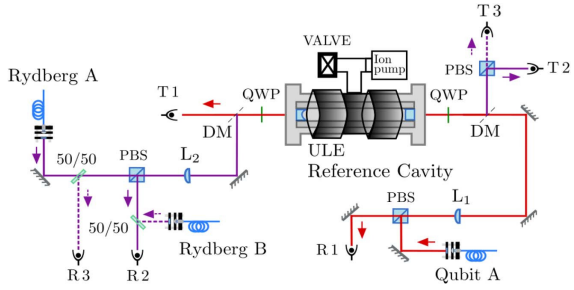

Fig. 2. Cavity locking setup used to lock two Rydberg lasers A and B (1018 nm) and the Qubit A laser (852 nm) to an ULE reference optical cavity with a fast Pound–Drever–Hall lock. Key: L, cavity mode-matching lens; DM, dichroic mirror; PBS, polarizing beam splitter; QWP, quarter-wave plate; R, high-bandwidth photodiode; T, high-gain photodiode.

As the cavity resonances are not necessarily commensurate with frequencies required for Rydberg excitation, we employ the "electronic sideband" technique [49,50] to provide a continuously tunable offset from the cavity modes of the two Rydberg lasers. A second frequency, ν_{Offset}, is amplified to +25 dBm and combined on a splitter with the low frequency PDH signal, ν_{PDH}, to drive the EOM with dual frequencies resulting in large first-order sidebands at $\pm\nu_{Offset}$, each of which has secondary PDH sidebands to enable locking. Through choice of phase in the PDH error signal, the laser can be locked to either the +1 or −1 sideband to achieve a frequency shift of $\mp\nu_{Offset}$ on the master laser with respect to the cavity. The offset frequency is derived from a DDS (AD9910) operating from 0.1 Hz to 460 MHz, which gives a tuning range of ±920 MHz after doubling.

4. SYSTEM PERFORMANCE

To evaluate the performance of the laser stabilization system, we first characterize the ULE cavity using an optical beat note between the 852 nm Qubit A laser and a second independent laser stabilized to the $6s_{1/2}F = 4 \rightarrow 6p_{3/2}F' = 5$ cooling transition using polarization spectroscopy [51]. Recording the beat note frequency as a function of cavity temperature, as shown in Fig. 3(a), results in a quadratic dependence due to the vanishing first-order coefficient of thermal expansion of the ULE cavity spacer [30]. Due to the large thermalization time constant of the cavity (measured to be approximately 12 h), each data point has been taken after a minimum period of 18 h following a change in temperature and up to 48 h later. From the data we extract the temperature of the zero-CTE crossing as $T_c = 36.1 \pm 0.1$°C. Following temperature stabilization of the cavity length at T_c, the free spectral range is measured by locking the laser to adjacent longitudinal cavity mode, as shown in Fig. 3(b). These data give

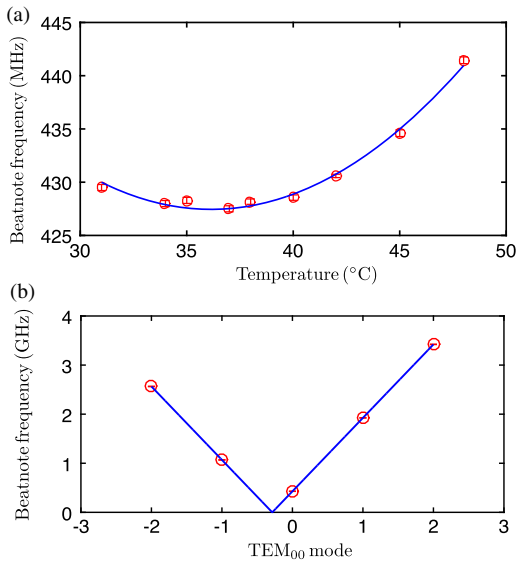

Fig. 3. (a) Determination of the zero-expansion temperature $T_c = 36.1 \pm 0.1$°C with a parabolic fit. Operating at T_c gives a second-order frequency sensitivity to temperature change. (b) Free spectral range determination via the beat note between Qubit A and a laser stabilized to the $F = 4$ to $F' = 5$ transition.

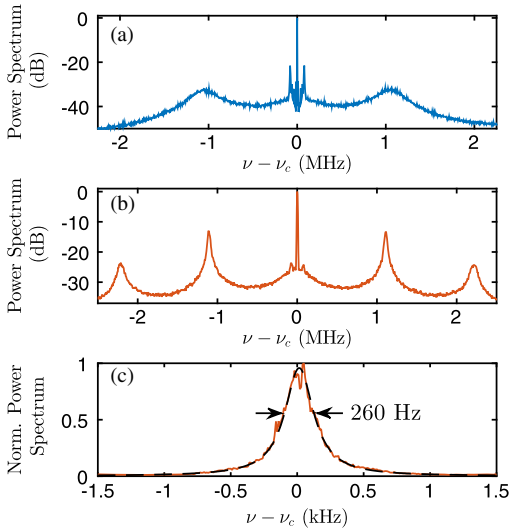

Fig. 4. (a) In-loop error signal for Rydberg B plotted relative to the PDH frequency with 5 kHz resolution bandwidth (RBW) showing servo bandwidth of 1.1 MHz. (b) Optical beat note relative to $\nu_c = 440$ MHz recorded at 509 nm between Rydberg A and B locked to consecutive TEM_{00} and TEM_{01} modes with 10 kHz RBW. (c) Linearized power spectrum recorded with 10 Hz RBW showing Lorentzian linewidth FWHM = 260(5) Hz. Data represent 100 rms averages using 190 ms sweep time.

$\nu_{FSR} = 1.49637(2)$ GHz, corresponding to a cavity length of $L = 10.0173(1)$ cm.

Cavity finesse is measured using cavity ring-down, where an AOM is used to rapidly extinguish light incident on the cavity resulting in an exponential decay of the transmitted light with a $1/e$ time constant equal to $\tau = \mathcal{F}/(2\pi\nu_{FSR})$ [52]. We record a time constant of $\tau = 15.1(9)$ μs at 852 nm, resulting in a finesse $\mathcal{F} = 1.42(8) \times 10^5$ and cavity linewidth $\delta\nu = 10.5$ kHz. As expected from the coating specification, at 1018 nm a reduced time constant of 4.1(4) μs is measured, corresponding $\mathcal{F} = 3.9(4) \times 10^4$ and $\delta\nu = 38.5$ kHz.

To evaluate the performance of the lock electronics, we measure the in-loop photodiode signal using an RF spectrum analyzer, as shown in Fig. 4(a) for Rydberg A. Either side of the central feature we observe a pair of high frequency servo-bumps at 1.1 MHz, corresponding to the bandwidth of fast current feedback

Direct measurement of laser linewidth for sub-kHz lasers is challenging and requires either multiple stable lasers, a narrow atomic reference, or a sufficiently long optical fiber to perform delayed self-heterodyne interferometry [53]. At 852 nm we are unable to perform either comparison; however, using the two Rydberg lasers A and B the linewidth can be measured from an optical beat note at 509 nm. Rydberg A is locked to the TEM_{00} mode of the ULE cavity while Rydberg B is locked to the TEM_{01}, with a frequency spacing of 220 MHz in the infrared. Figures 4(b) and 4(c) show the optical beat note recorded on an rf spectrum analyzer with each trace the RMS average of 100 shots recorded with a 190 ms sweep time. Figure 4(b) reveals secondary peaks at harmonics of 1.1 MHz corresponding to the fast-feedback servo bumps for each laser. Fitting the central peak to a Lorentzian in Fig. 4(c) returns a linewidth of 260(5) Hz relative to the cavity, from which we can estimate a linewidth of ∼130 Hz for each laser due to the fact that both lasers are locked using identical components. While this measurement may underestimate the linewidth due to common mode noise rejection from locking to a single cavity, this results in an IR linewidth <100 Hz with better performance expected at 852 nm due to the increase in cavity finesse at this wavelength and an increased servo bandwidth of 1.2 MHz.

Converting the observed laser linewidth to gate fidelity is complex due to the error in a two-photon Raman transition being related to the relative phase noise between the two lasers [54], which due to their different wavelengths cannot be measured without performing gate operations on a single qubit. As the lasers are locked to a common cavity the fluctuations are also correlated, meaning the linewidths are not additive. However, using the available laser power an effective two-photon Rabi frequency of $\Omega/2\pi = 10$ MHz can be achieved with a few gigahertz intermediate state detuning [11]. For a relative linewidth of 100 Hz, this results in an averaged gate error $\varepsilon \simeq 10^{-6}$ when modeling the linewidth as a dephasing term following [55]. Thus, the laser system is suitable for high-fidelity gates, with the laser-limited coherence time greatly exceeding the gate duration.

5. ATOMIC SPECTROSCOPY—RYDBERG EIT

To calibrate ULE cavity mode frequencies with respect to Rydberg transitions we have performed high-resolution spectroscopy on a cold atomic ensemble using Rydberg EIT [12,56]. Measurements are performed using the $50S_{1/2}$ Rydberg state to reduce sensitivity to stray electric fields and minimize interaction effects. This is chosen as one of the lowest

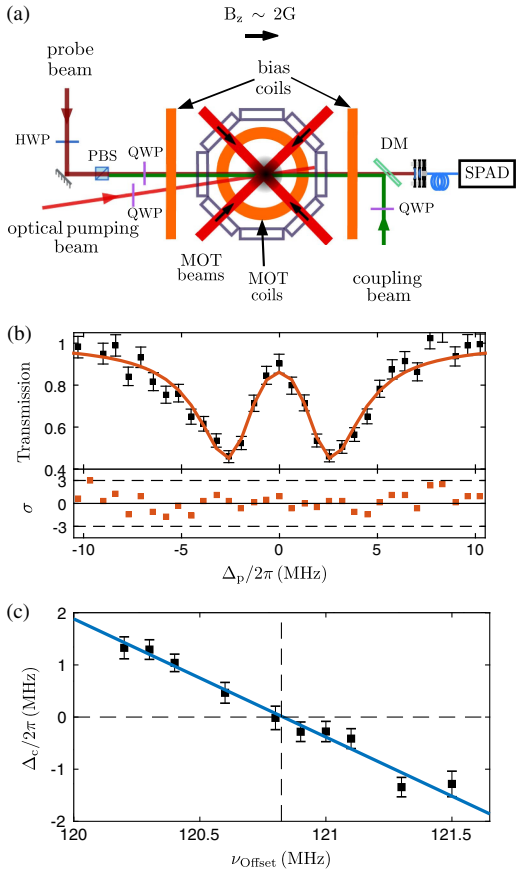

Fig. 5. (a) Schematic of the experimental EIT setup. A strong coupling beam (green) counter-propagates with a weak probe beam (red) through a cold atom cloud of Cs atoms optically pumped in the $|F = 4, m_F = 4\rangle$ dark state. (b) EIT transmission peak for $50S_{1/2}$ Rydberg state with a coupling power of 50 mW with fitted $\chi^2_\nu = 1.0$. Error bars represent one standard deviation. (c) Coupling laser detuning $\Delta_c/2\pi$ as a function of the coupling laser offset frequency, fitted according to the formula $\Delta_c/2\pi = \alpha(\nu_{Offset} - \nu_0)$, showing the two-photon resonance at $\nu_0 = 120.82(4)$ MHz.

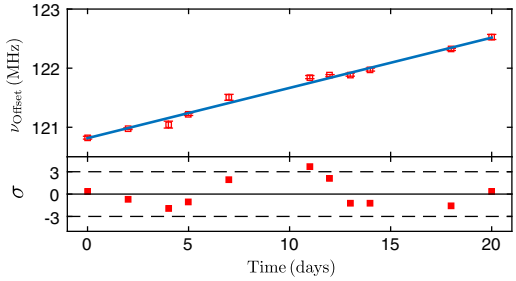

Fig. 6. EIT resonance's frequency of $50S_{1/2}$ Rydberg state recorded for a period of 20 days. Using a linear fit, the constant cavity's drift is evaluated at 1 Hz/s. Inset shows normalized residuals. Error bars reflect standard errors.

n levels accessible with the current setup. Experiments are performed on a laser-cooled ^{133}Cs atom cloud with the experimental setup shown schematically in Fig. 5(a). Atoms are loaded into a magneto-optical trap for 1 s followed by a short polarization gradient cooling stage resulting in 10^5 atoms at a temperature of 5 μK. Atoms are then prepared in the $|F = 4, m_F = 4\rangle$ stretched state by dark-state optical pumping with σ^+ polarized light on the $6S_{1/2}F = 4 \rightarrow 6P_{3/2}F' = 4$ transition using a 2 G magnetic field along the probe beam to define a quantization axis.

EIT spectroscopy is performed using counter-propagating probe and coupling lasers focused to $1/e^2$ radii of 13 μm and 84 μm, respectively. The probe laser is derived from the cooling laser, stabilized using polarization spectroscopy on the $6s^2S_{1/2} \rightarrow 6p^2P_{3/2}$ transition. The coupling laser, Rydberg B, is offset-locked to the cavity and drives the $6p^2P_{3/2} \rightarrow 50s^2S_{1/2}$ with a power of 50 mW. The probe and coupling lasers are circularly polarized in a $\sigma^+ - \sigma^-$ configuration with respect to the quantization axis, maximizing the transition amplitude to the Rydberg state. The probe power is fixed at 0.5 pW ($I/I_{sat} \sim 5 \times 10^{-4}$) and the probe transmission is recorded using a single photon counting module. For each measurement, the probe laser is scanned across the resonance from $\Delta_p/2\pi = -12 \rightarrow +12$ MHz in 1 ms, with spectra recorded from the average of 100 shots. Data are recorded as a function of the coupling laser offset frequency, ν_{Offset}, to find the resonant frequency for the upper transition with respect to the cavity resonance.

Figure 5(b) shows a typical EIT spectrum for a sideband frequency $\nu_{Offset} = 120.8$ MHz, which is fit to the weak-probe susceptibility [55] enabling determination of the Rabi frequency, $\Omega_c/2\pi = 5.1(2)$ MHz, and the coupling laser detuning Δ_c. Error bars represent one standard deviation. The normalized residuals on the lower panel show excellent agreement between theory and experiment, with $\chi^2_\nu = 1.0$. From the complete set of spectra, the coupling laser detuning as a function of sideband frequency is plotted in Fig. 5(c) and fit using the formula $\Delta_c = \alpha(\nu_{Offset} - \nu_0)$, enabling determination of the resonant sideband frequency as $\nu_0 = 120.82(4)$ MHz with a precision of less than 0.1 MHz.

Using this high-resolution method to extract the resonant transition frequency, we repeat the EIT spectroscopy over a period of 20 days to determine the long-term frequency drift of the cavity with respect to the atomic transition, as shown in Fig. 6. The results show an average linear frequency drift of 1 Hz/s, confirming the ULE cavity is optimized close to the zero-CTE temperature but still limited by creep of the spacer or outgassing in the ULE cavity vacuum.

6. CONCLUSION

We have demonstrated sub-kHz linewidth lasers for Rydberg excitation with three lasers locked simultaneously to the same high-finesse ULE reference cavity. The lock configuration allows continuous tuning of the laser offset using the "electronic sideband" technique, and after frequency doubling we measure laser linewidth of ~130 Hz at 509 nm suitable for performing high-fidelity quantum gates. Using high-resolution EIT spectroscopy on a cold atom cloud, we calibrate cavity frequencies with respect to Rydberg transitions with a precision of <0.1 MHz. Finally, we have demonstrated excellent long-term stability with a linear drift of ~1 Hz/s relative to an atomic reference. These measurements are competitive against

doubly stabilized optical clocks [32,37] and offer an order of magnitude improvement compared to similar cavity-stabilized Rydberg laser systems [35,36].

Funding. Engineering and Physical Sciences Research Council (EPSRC) (EP/N003527/1).

Acknowledgment. We acknowledge Erling Riis for useful discussions and careful reading of the paper. The data presented in the paper are available for download [57].

REFERENCES

1. M. A. Nielsen and I. L. Chuang, *Quantum Computation and Quantum Information* (Cambridge University, 2005).
2. M. Saffman, "Quantum computing with atomic qubits and Rydberg interactions: progress and challenges," J. Phys. B **49**, 202001 (2016).
3. J. M. Auger, S. Bergamini, and D. E. Browne, "Blueprint for fault-tolerant quantum computation with Rydberg atoms," Phys. Rev. A **96**, 052320 (2017).
4. P. Treutlein, P. Hommelhoff, T. Steinmetz, T. Hänsch, and J. Reichel, "Coherence in microchip traps," Phys. Rev. Lett. **92**, 203005 (2004).
5. M. Saffman, T. G. Walker, and K. Mølmer, "Quantum information with Rydberg atoms," Rev. Mod. Phys. **82**, 2313–2363 (2010).
6. T. Wilk, A. Gaëtan, C. Evellin, J. Wolters, Y. Miroshnychenko, P. Grangier, and A. Browaeys, "Entanglement of two individual neutral atoms using Rydberg blockade," Phys. Rev. Lett. **104**, 010502 (2010).
7. Y.-Y. Jau, A. M. Hankin, T. Keating, I. H. Deutsch, and G. W. Biedermann, "Entangling atomic spins with a Rydberg-dressed spin-flip blockade," Nat. Phys. **12**, 71–74 (2016).
8. L. Isenhower, E. Urban, X. L. Zhang, A. T. Gill, T. Henage, T. A. Johnson, T. G. Walker, and M. Saffman, "Demonstration of a neutral atom controlled-NOT quantum gate," Phys. Rev. Lett. **104**, 010503 (2010).
9. K. M. Maller, M. T. Lichtman, T. Xia, Y. Sun, M. J. Piotrowicz, A. W. Carr, L. Isenhower, and M. Saffman, "Rydberg-blockade controlled-not gate and entanglement in a two-dimensional array of neutral-atom qubits," Phys. Rev. A **92**, 022336 (2015).
10. H. Labuhn, D. Barredo, S. Ravets, S. de Léséleuc, T. Macr, T. Lahaye, and A. Browaeys, "Tunable two-dimensional arrays of single Rydberg atoms for realizing quantum Ising models," Nature **534**, 667–670 (2016).
11. T. A. Johnson, E. Urban, T. Henage, L. Isenhower, D. D. Yavuz, T. G. Walker, and M. Saffman, "Rabi oscillations between ground and Rydberg states with dipole-dipole atomic interactions," Phys. Rev. Lett. **100**, 113003 (2008).
12. A. K. Mohapatra, T. R. Jackson, and C. S. Adams, "Coherent optical detection of highly excited Rydberg states using electromagnetically induced transparency," Phys. Rev. Lett. **98**, 113003 (2007).
13. R. P. Abel, A. K. Mohapatra, M. G. Bason, J. D. Pritchard, K. J. Weatherill, U. Raitzsch, and C. S. Adams, "Laser frequency stabilization to excited state transitions using electromagnetically induced transparency in a cascade system," Appl. Phys. Lett. **94**, 071107 (2009).
14. M. Mack, F. Karlewski, H. Hattermann, S. Höckh, F. Jessen, D. Cano, and J. Fortágh, "Measurement of absolute transition frequencies of ^{87}Rb to nS and nD Rydberg states by means of electromagnetically induced transparency," Phys. Rev. A **83**, 052515 (2011).
15. J. Grimmel, M. Mack, F. Karlewski, F. Jessen, M. Reinschmidt, N. Sándor, and J. Fortágh, "Measurement and numerical calculation of Rubidium Rydberg Stark spectra," New J. Phys. **17**, 053005 (2015).
16. M. Mack, J. Grimmel, F. Karlewski, L. M. H. Sárkány, H. Hattermann, and J. Fortágh, "All-optical measurement of Rydberg-state lifetimes," Phys. Rev. A **92**, 012517 (2015).
17. A. Tauschinsky, R. M. T. Thijssen, S. Whitlock, H. B. van Linden van den Heuvell, and R. J. C. Spreeuw, "Spatially resolved excitation of Rydberg atoms and surface effects on an atom chip," Phys. Rev. A **81**, 063411 (2010).
18. J. A. Sedlacek, A. Schwettmann, H. Kübler, R. Löw, T. Pfau, and J. P. Shaffer, "Microwave electrometry with Rydberg atoms in a vapour cell using bright atomic resonances," Nat. Phys. **8**, 819–824 (2012).
19. H. Fan, S. Kumar, J. Sedlacek, H. Kübler, S. Karimkashi, and J. P. Shaffer, "Atom based RF electric field sensing," J. Phys. B **48**, 202001 (2015).
20. C. G. Wade, N. Šibalić, N. R. de Melo, J. M. Kondo, C. S. Adams, and K. J. Weatherill, "Real-time near-field terahertz imaging with atomic optical fluorescence," Nat. Photonics **11**, 40–43 (2017).
21. J. D. Pritchard, K. J. Weatherill, and C. S. Adams, "Non-linear optics using cold Rydberg atoms," Annu. Rev. Cold Atoms Mol. **1**, 301–350 (2013).
22. O. Firstenberg, C. S. Adams, and S. Hofferberth, "Nonlinear quantum optics mediated by Rydberg interactions," J. Phys. B **49**, 152003 (2016).
23. H. Gorniaczyk, C. Tresp, P. Bienias, A. Paris-Mandoki, W. Li, I. Mirgorodskiy, H. P. Büchler, I. Lesanovsky, and S. Hofferberth, "Enhancement of Rydberg-mediated single-photon nonlinearities by electrically tuned Förster resonances," Nat. Commun. **7**, 12480 (2016).
24. D. Tiarks, S. Schmidt, G. Rempe, and S. Dürr, "Optical π phase shift created with a single-photon pulse," Sci. Adv. **2**, e1600036 (2016).
25. H. K. Cummins, G. Llewellyn, and J. A. Jones, "Tackling systematic errors in quantum logic gates with composite rotations," Phys. Rev. A **67**, 042308 (2003).
26. R. W. Fox, C. W. Oates, and L. W. Hollberg, "Stabilizing diode lasers to high-finesse cavities," Exp. Methods Phys. Sci. **40**, 1–46 (2003).
27. M. J. Martin and J. Ye, *Optical Coatings and Thermal Noise in Precision Measurement* (Cambridge University, 2012), Chap. 15, p. 237.
28. B. J. Bloom, T. L. Nicholson, J. R. Williams, S. L. Campbell, M. Bishof, X. Zhang, W. Zhang, S. L. Bromley, and J. Ye, "An optical lattice clock with accuracy and stability at the 10^{-18} level," Nature **506**, 71–75 (2014).
29. S. L. Campbell, R. B. Hutson, G. E. Marti, A. Goban, N. Darkwah Oppong, R. L. McNally, L. Sonderhouse, J. M. Robinson, W. Zhang, B. J. Bloom, and J. Ye, "A Fermi-degenerate three-dimensional optical lattice clock," Science **358**, 90–94 (2017).
30. J. Alnis, A. Matveev, N. Kolachevsky, T. Udem, and T. W. Hänsch, "Subhertz linewidth diode lasers by stabilization to vibrationally and thermally compensated ultralow-expansion glass Fabry–Perot cavities," Phys. Rev. A **77**, 053809 (2008).
31. G. Cappellini, P. Lombardi, M. Mancini, G. Pagano, M. Pizzocaro, L. Fallani, and J. Catani, "A compact ultranarrow high-power laser system for experiments with 578 nm ytterbium clock transition," Rev. Sci. Instrum. **86**, 073111 (2015).
32. I. R. Hill, R. Hobson, W. Bowden, E. M. Bridge, S. Donnellan, E. A. Curtis, and P. Gill, "A low maintenance Sr optical lattice clock," J. Phys. Conf. Ser. **723**, 012019 (2016).
33. C. Hagemann, C. Grebing, C. Lisdat, S. Falke, T. Legero, U. Sterr, F. Riehle, M. J. Martin, and J. Ye, "Ultrastable laser with average fractional frequency drift rate below 5×10^{19}/s," Opt. Lett. **39**, 5102–5105 (2014).
34. D. G. Matei, T. Legero, S. Häfner, C. Grebing, R. Weyrich, W. Zhang, L. Sonderhouse, J. M. Robinson, J. Ye, F. Riehle, and U. Sterr, "1.5 μm lasers with sub-10 mHz linewidth," Phys. Rev. Lett. **118**, 263202 (2017).
35. A. Arias, S. Helmrich, C. Schweiger, L. Ardizzone, G. Lochead, and S. Whitlock, "Versatile, high-power 460 nm laser system for Rydberg excitation of ultracold potassium," Opt. Express **25**, 14829–14839 (2017).
36. J. de Hond, N. Cisternas, G. Lochead, and N. J. van Druten, "Medium-finesse optical cavity for the stabilization of Rydberg lasers," Appl. Opt. **56**, 5436–5443 (2017).
37. E. M. Bridge, N. C. Keegan, A. D. Bounds, D. Boddy, D. P. Sadler, and M. P. A. Jones, "Tunable cw UV laser with <35 kHz absolute frequency instability for precision spectroscopy of Sr Rydberg states," Opt. Express **24**, 2281–2292 (2016).
38. A. S. Arnold, J. S. Wilson, and M. G. Boshier, "A simple extended-cavity diode laser," Rev. Sci. Instrum. **69**, 1236–1239 (1998).

39. A. Hemmerich, D. H. McIntyre, C. Zimmermann, and T. W. Hänsen, "Second-harmonic generation and optical stabilization of a diode laser in an external ring resonator," Opt. Lett. **15**, 372–374 (1990).
40. G. D. Boyd and D. A. Kleinman, "Parametric interaction of focused Gaussian light beams," J. Appl. Phys. **39**, 3597–3639 (1968).
41. T. Hansch and B. Couillaud, "Laser frequency stabilization by polarization spectroscopy of a reflecting reference cavity," Opt. Commun. **35**, 441–444 (1980).
42. A. G. White, P. K. Lam, M. S. Taubman, M. A. M. Marte, S. Schiller, D. E. McClelland, and H.-A. Bachor, "Classical and quantum signatures of competing $\chi^{(2)}$ nonlinearities," Phys. Rev. A **55**, 4511–4515 (1997).
43. I. Ricciardi, M. D. Rosa, A. Rocco, P. Ferraro, and P. D. Natale, "Cavity-enhanced generation of 6 W cw second-harmonic power at 532 nm in periodically-poled MgO:$LiTaO_3$," Opt. Express **18**, 10985–10994 (2010).
44. R. L. Targat, J.-J. Zondy, and P. Lemonde, "75%-efficiency blue generation from an intracavity PPKTP frequency doubler," Opt. Commun. **247**, 471–481 (2005).
45. R. W. P. Drever, J. L. Hall, F. V. Kowalski, J. Hough, G. M. Ford, A. J. Munley, and H. Ward, "Laser phase and frequency stabilization using an optical resonator," Appl. Phys. B **31**, 97–105 (1983).
46. E. D. Black, "An introduction to Pound-Drever-Hall laser frequency stabilization," Am. J. Phys. **69**, 79–87 (2001).
47. R. W. Fox, "Temperature analysis of low-expansion Fabry–Perot cavities," Opt. Express **17**, 15023–15031 (2009).
48. L. Chen, J. L. Hall, J. Ye, T. Yang, E. Zang, and T. Li, "Vibration-induced elastic deformation of Fabry–Perot cavities," Phys. Rev. A **74**, 053801 (2006).
49. J. I. Thorpe, K. Numata, and J. Livas, "Laser frequency stabilization and control through offset sideband locking to optical cavities," Opt. Express **16**, 15980–15990 (2008).
50. P. D. Gregory, P. K. Molony, M. P. Köppinger, A. Kumar, Z. Ji, B. Lu, A. L. Marchant, and S. L. Cornish, "A simple, versatile laser system for the creation of ultracold ground state molecules," New J. Phys. **17**, 055006 (2015).
51. C. P. Pearman, C. S. Adams, S. G. Cox, P. F. Griffin, D. A. Smith, and I. G. Hughes, "Polarization spectroscopy of a closed atomic transition: applications to laser frequency locking," J. Phys. B **35**, 5141–5151 (2002).
52. G. Rempe, R. Lalezari, R. J. Thompson, and H. J. Kimble, "Measurement of ultralow losses in an optical interferometer," Opt. Lett. **17**, 363–366 (1992).
53. T. Okoshi, K. Kikuchi, and A. Nakayama, "Novel method for high resolution measurement of laser output spectrum," Electron. Lett. **16**, 630–631 (1980).
54. M. Saffman and T. G. Walker, "Analysis of a quantum logic device based on dipole-dipole interactions of optically trapped Rydberg atoms," Phys. Rev. A **72**, 022347 (2005).
55. J. Gea-Banacloche, Y. Li, S. Jin, and M. Xiao, "Electromagnetically induced transparency in ladder-type inhomogeneously broadened media: theory and experiments," Phys. Rev. A **51**, 576–584 (1995).
56. J. D. Pritchard, D. Maxwell, A. Gauguet, K. J. Weatherill, M. P. A. Jones, and C. S. Adams, "Cooperative atom-light interaction in a blockaded Rydberg ensemble," Phys. Rev. Lett. **105**, 193603 (2010).
57. R. Legaie, C. J. Picken, and J. D. Pritchard, "Data for 'sub-kHz excitation lasers for quantum information processing with Rydberg atoms'," arXiv:1711.02645v1 (2017).